Arabian Journal for Science and Engineering
https://doi.org/10.1007/s13369-024-09182-4

RESEARCH ARTICLE-CIVIL ENGINEERING

Design and Nonlinear Dynamic Response of a Steel Stack

Cuneyt Vatansever[1] · **Hasim Cayir**[1,2]

Received: 4 March 2024 / Accepted: 12 May 2024

Abstract
Industrial stacks are built in order to reduce atmospheric pollution and release gases to the higher level of the atmosphere. Since they are high and slender structures, they are significantly affected by lateral forces, in particular, induced by winds and earthquakes. This paper aims to summarize the design principles for steel stacks given in the international standards, codes and specifications considering the evaluation of the results from the investigation on nonlinear dynamic response of a typical steel stack subjected to the earthquake. For this purpose, a typical self-supporting steel stack has been designed and its performance under earthquake and wind forces has been investigated in terms of the applied design principles, such as the displacement limit and the potential plastic deformations. The study is accomplished by using finite element models employing nonlinear time history and pushover analyses. The numerical results are presented particularly by considering the design principles used for the model. The results show that wind loads considered are more pronounced in the design of industrial steel stacks than earthquake especially in terms of limiting top displacement. The flue openings which reduce strength and lateral stiffness of the stack web is significantly effective in the lateral behavior of the stack. Moreover, the principles considered are found applicable for the design of such steel stacks. Based on the results from nonlinear time history analyses, no yielding and plastic deformation are detected along the stack.

Keywords Steel stack · Nonlinear time history analysis · Pushover analysis · Seismic response · Wind load · Vortex shedding · Finite element analysis

1 Introduction

Industrial steel stacks are structural elements that carry harmful smoke, soot, dust, steam, and gases formed in industrial facilities to high levels of the atmosphere in order not to pollute the air we breathe and thus aim to prevent environmental pollution. The construction of tall stacks has been started with this increasing awareness of preventing air pollution caused by industrial facilities. Given the existing industrial chimneys, it is seen that building materials such as masonry, reinforced concrete and steel are used in their construction. In recently built chimneys, reinforced concrete and steel have been used instead of masonry, except for special cases.

Although chimneys do not pose a great danger to life like the highly populated buildings, damage to these structures can result in the closure of facilities and industries. Therefore, it is important that the chimneys have to be designed so as to serve their function properly without experiencing significant damage and collapse.

As the industrial chimneys are high and slender structures, they have different structural problems and should be addressed separately from other tower structures. Due to their structural system, earthquake and wind are the two most important effects in the design of the chimneys.

Studies on industrial steel stacks generally focus on the stack's behavior under wind loads. However, there are not many studies on the performance of the steel stack. Gaczek et al. [1] reported that the largest top displacement of the steel stack was caused by wind loads. Moreover, they investigated the effects of helical strakes on the cross-wind vibrations. The use of helical strakes was emphasized to damp the cross-wind oscillation, which in turn reduced the displacements induced by cross-wind effect.

Kawecki et al. [2] examined different approaches accounted for the effect of damping on cross-wind vibration of steel chimneys due to the vortex excitation and the

✉ Hasim Cayir
hcayir@fsm.edu.tr

[1] Department of Civil Engineering, Istanbul Technical University, 34469 Maslak, Istanbul, Turkey

[2] Department of Civil Engineering, Fatih Sultan Mehmet Vakif University, 34445 Beyoglu, Istanbul, Turkey

Published online: 04 June 2024

effect of Scruton number on the relative amplitude of vibration, considering Eurocode 1 [3] and CICIND [4] standards. They also demonstrated that climatic conditions significantly affect the vibrations of the steel chimney.

Susuki et al. [5] studied the behavior of a 200 m-high tower-supported steel stack under wind-induced vibration. The effect of the tuned mass damper on vortex-induced vibrations was investigated by long-term observation, a man-powered vibration test and a wind tunnel test. It was emphasized that vortex-induced vibration was significantly reduced with the use of tuned mass damper in the steel stack.

Huang et al. [6] investigated a 115-m high reinforced concrete chimney that collapsed at the Tüpraş Refinery during the 17 August 1999 Izmit Earthquake by using the linear response spectrum analysis method and the nonlinear static pushover analysis by employing the finite element method with finite element analysis software ABAQUS [7, 8]. The effect of flue openings on the behavior was investigated and the capacity curve was obtained. It was confirmed that the actual collapse consequence and that of the model were compatible with each other.

The weakest section of most of the reinforced concrete chimneys exposed to severe earthquakes is flue opening near the base of the chimney. Wilson [9] experimentally investigated the behavior of a reinforced concrete chimney under cyclic loading, which includes bending critical and shear critical sections at the openings. The parameters such as failure mode, overstrength factor, available ductility, hysteretic behavior and strain distribution were examined. It is shown that the presence of the flue openings decreases the ductility of the chimneys significantly.

The aim of this study is to design a self-supported steel stack, which is highly preferred in industry and power generation facilities and to investigate its performance under lateral forces by performing the static pushover analysis and the nonlinear time history analysis. The applicability of applied design principles is examined in the direction of the analyses results. The effect of flue opening is also investigated in terms of the lateral stiffness and the strength of the stack. Additionally, a contribution to current literature lacking of investigating the seismic behavior of self-supported steel stack has been aimed.

2 Design of a Typical Steel Stack

During the design of the sample self-supporting steel stack, different codes and specifications, such as ASME STS-1 [10], Eurocode 1, Eurocode 3 [11], IS 6533 [12], CICIND, ASCE 7-16 [13] and AISC 360-16 [14] have been considered. Given that each individual code and specification cannot be expected to include all subjects, it is found to be worth to establish a design procedure including almost all requirements that need to be satisfied for the design of a steel stack. No any inconsistency among the requirements applied from different codes and specifications was allowed in the establishment of design procedure which is clearly explained in the following sections.

Table 1 Characteristics of steel material

Modulus of elasticity, E [GPa]	200
Poisson's ratio, ν	0.3
Density, ρ [kg/m^3]	7850
Yield strength, F_y [MPa]	235
Ultimate strength, F_u [MPa]	360

The steel grade of S235 was used as the material of the sample self-supporting steel stack. The basic mechanical properties of the steel material are shown in Table 1. The steel stack consists of five individual segments with cross sections having outside diameters vary along its height while inner diameter of 3.30 m is constant. The total height of the stack is 60.65 m. The height is 12 m in the first four sections and 12.65 m in the last section. The thicknesses of cylindrical shells, decreasing from the bottom to the top for each part, is as follows: 25 mm, 20 mm, 15 mm, 12 mm and 10 mm, respectively. The geometric features of the stack are shown in Fig. 1a. The stack was modeled using shell elements in the structural software of SAP2000 [15] as seen in Fig. 1b.

Dead loads were composed of self-weight of the stack and own weight of the steel platforms. The areas of the platforms built at the heights of 41.00 m and 58.65 m are 38.18 m^2 and 17.04 m^2, respectively. The own weight of the platforms was considered by adding 0.50 kN/m^2 to the self-weight of the stack at the levels of 41.00 m and 58.65 m where the platforms are located.

Temporary loads likely to occur during maintenance and renovation are considered as live loads. The loads suggested in the codes as a live load for the platforms and walkways are as follows:

i—Minimum 2.40 kN/m^2 (50 psf) in ASME STS-1,
ii—2.0 kN/m^2 in Eurocode 3,
iii—3.0 kN/m^2 in IS 6533.

In the design of the stack, live load was taken as 2.50 kN/m^2 which is approximately equal to that stated in the ASME-STS-1. The live load was added in the load combinations including the seismic and the wind effects although the ASME-STS-1 stipulates that it need not to be considered in the combinations.

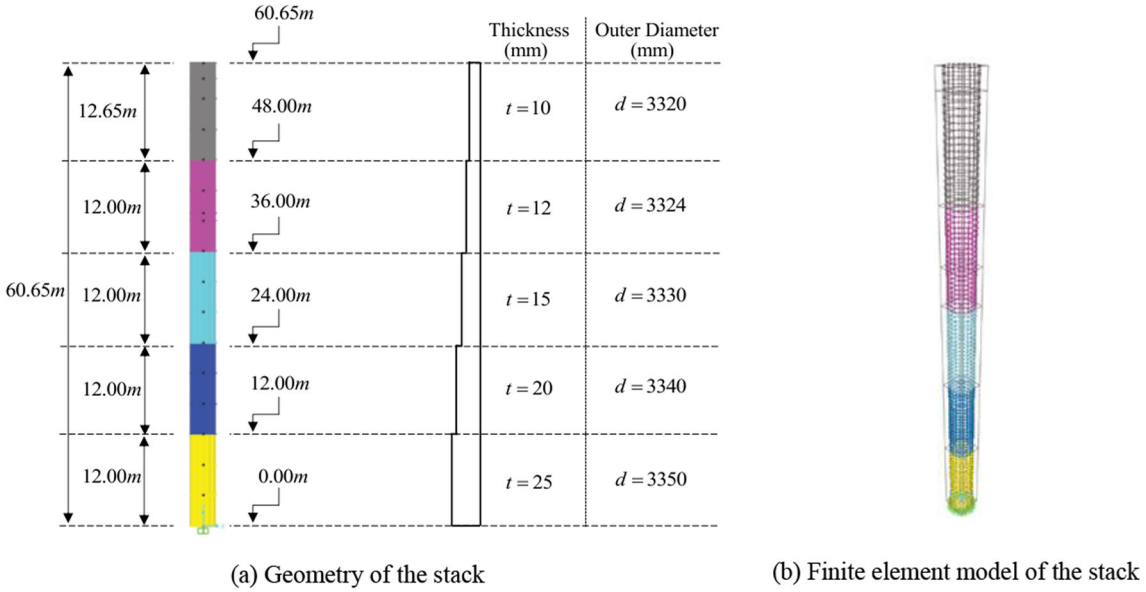

(a) Geometry of the stack

(b) Finite element model of the stack

Fig. 1 Dimensional properties and FEM of the stack

2.1 Thermal Effect

Steel is a very sensitive structural material to heat. As the temperature increases, it loses its strength and the modulus of elasticity can decrease rapidly. If no precautions are taken, the structural steel starts to soften and lose its strength at high temperatures, which causes geometry changes. High temperature causes significant changes in the mechanical properties of structural steel elements and significant expansion. Experiments have shown that the yield point of carbon steel decreases as the temperature increases [16]. Therefore, structural steel members must be protected against high temperatures.

Non-uniform distribution of flue gas along the steel stack and temperature differences between the stack shells cause thermal stresses in both longitudinal and circumferential directions. If the stack is exposed to high temperature (> 260 °C), the effect of temperature must be considered in the design and localized thermal stresses induced in the inner plates and stiffeners can be substantial and must be considered load combination according to ASME-STS-1. For temperatures exceeding 400 °C, the effects of temperature creep should be considered to avoid creep rupture. The aluminum coating and lining can be applied (IS 6533). In this paper, the temperature was assumed to be low enough (< 260 °C), thus the effect of the thermal stresses was negligible. For more discussion of the thermal effects, it can be referred to Design and Construction of Steel Stack Liners [17].

IS 6533 accounts for the thermal effect using a temperature coefficient. It does not allow the most critical stress obtained from the load combinations to exceed the maximum permissible stresses, which is given in the code depending on the ratio of the diameter to the thickness of the steel stack. Maximum permissible stresses are expected to be evaluated for the most adverse temperature conditions to which the member or part may reasonably be expected to be exposed by multiplying with the appropriate temperature coefficient K_t given in the code. In addition, the expected flue temperature is not allowed to exceed 400 °C. In this paper, the flue temperature was assumed to be between 0 and 200 °C and thus, no reduction in the permissible stresses was applied by taking $K_t = 1.0$.

2.2 Seismic Effect

In the codes, the use of response spectrum method for determining the response of steel stacks to earthquake is recommended, additionally ASME-STS-1 states that a static equivalent method can be used. Seismic loads were determined according to the Turkish Seismic Code for Buildings (TSCB) 2018 [18] which have basically a close resemblance to the ASCE 7-16. Both equivalent earthquake load method and response spectrum method were used to determine the seismic load for the steel stack and the results were compared.

The steel stack is assumed to be located in Balikesir/Turkey, a region of high seismicity. The corresponding acceleration coefficients for the short period $S_S = 0.869$ g ($S_{DS} = 1.001$ g including site soil class modification factor) and the spectral coefficient (for the period for 1 s) $S_1 = 0.216$ g ($S_{D1} = 0.468$ g including site soil class modification factor) are assumed for the design earthquake. The mass of the steel stack is found to be 83.86 kN-s^2/m (ton).

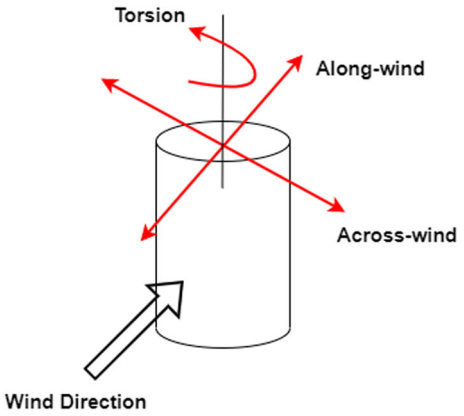

Fig. 2 Wind load directions on a circular structure

Furthermore, as the response modification factor and the overstrength factor are not stated in TSCB 2018 for steel stacks, these factors adapted from ASCE 7–16 were as assumed to be 2.0 and 2.0, respectively. The building importance factor (I) of 1.0 and the site soil class ZD were adopted according to the TSCB 2018. Under these assumptions, the unreduced base shear force with the seismic load reduction factor considered during the design is as follows for the equivalent earthquake load method and the response spectrum method, 576 kN and 552 kN, respectively.

2.3 Wind Effect

Steel stacks are subjected to bending and torsional oscillations in the across-wind direction, as well as in the along-wind direction under the influence of dynamic wind loads (Fig. 2). Across-wind and torsional vibrations of the stack are usually caused by vortex shedding, which acts on the side layers of the stack [19]. These vibrations caused by vortex shedding are very complex due to their natural behavior and require special investigation.

In the design wind loads that produce these vibrations are determined according to Eurocode 1. In the present design the fundamental value of the basic wind velocity is set to be 28 m/s, the construction area of the stack is considered to be Class III and the equivalent surface roughness is taken as 0.2. The total wind pressure which acts vertically at the outer surface of the stack was calculated on discrete points over the stack by using to Eurocode 1.

The effect of vibrations induced by vortex shedding was considered from the effect of the inertia force per unit length according to Equation (E.6) in Annex E.1 of Eurocode 1, acting perpendicular to the wind direction on the stack. The base shear forces calculated in the design stage are as follows for the along-wind direction and cross-wind direction, 285.04 kN and 1683.22 kN, respectively.

2.4 Limit States

Strength limit state of the steel stack was checked per ASME STS-1. Eurocode 3 and IS 6533 were considered to limit the lateral top displacement of the stack. ASME STS-1 does not specify any lateral displacement limit; however, it suggests that secondary stresses caused by $P{\cdot}\Delta$ and the foundation rotation or movement should be considered to determine the maximum lateral displacement. Eurocode 3 stipulates, depending on the safety level, that the maximum lateral top displacement of the stack in the across-wind direction can be limited to 10% of the outer diameter of the stack and that in the along-wind direction is limited to $\delta_{max} = h/50$, whereas IS 6533 specifies that the maximum lateral top displacement of the circular stack in along-wind direction is limited to $\delta_{max} = h/200$. Given the steel stack is a cantilever structure, the maximum lateral top displacement can be limited to $\delta_{max} = h/150$ adopted herein, in which "h" is the unsupported height of the steel stack.

Local buckling limit state was also checked according to the following equation suggested by Troitsky [20] which is based on allowable stress design method and obtained from a systematic evaluation of test evidence:

$$\sigma_{cr} = \frac{662}{D/t} + 0.399F_y$$

where σ_{cr} is permissible compressive stress in ksi, F_y is yield stress of the material in ksi and D/t is the ratio of the diameter to the thickness of the steel stack.

2.5 Load Combinations

Two similar approaches based on the allowable strength were addressed to establish the load combinations considered in the design. In the first approach, the load combinations given for the Allowable Strength Design (ASD) of the Turkish Code for Design and Construction of Steel Structures (TCDCSS) 2016 [21] which has a close resemblance to the AISC 360-16 were used. The load combinations established according to ASME STS-1 were introduced into the second approach, as shown in Table 2. G, Q, E, W_{along} and W_{across} given in Table 2 represent dead load, live load, seismic load, wind load along the wind direction and wind load across to the wind direction, respectively.

ASME STS-1 specifies that the stack shall be designed for the factor of safety of 1.50 to obtain the allowable stresses for the load combinations containing seismic or wind load. The safety factor was defined as 1.67 to achieve allowable stresses for a particular limit states associated with the ASD load combinations of the TCDCSS 2016 based on the relationship between Load and Resistance Factor Design Approach (LRFDA) and Allowable Strength Design

Table 2 Load combinations of ASME STS-1 and TCDCSS 2016

ASME STS-1	TCDCSS 2016
$G + Q + W_{along}$	$G + W_{along}$
	$G + 0.75Q + 0.75W_{along}$
$G + Q + W_{across}$	$G + W_{across}$
	$G + 0.75Q + 0.75W_{across}$
$G + Q + E$	$G + 0.7E$
	$G + 0.75Q + 0.75(0.7E)$

Table 3 The most critical displacement and its limit

	Load combination	Load combination approach	The maximum lateral top displacement (mm)	Limit (mm)
Without helical strake	$G + W_{across}$	TCDCSS 2016	1293	404
	$G + Q + W_{across}$	ASME STS-1	1297	
With helical strake	$G + W_{across}$	TCDCSS 2016	241	404
	$G + Q + W_{across}$	ASME STS-1	242	

Approach (ASDA). In order to ensure compatibility between the two approaches, normal service conditions associated with the load combinations appropriate for allowable strength design. More details can be found in AISC Steel Construction Manual 15th Edition [22].

2.6 Evaluation of the Results

Since in the present case, a relatively large wind load is adopted, the steel stack cannot satisfy the limit states due to the effect of large across-wind load assumed, when the effect of wind was not damped. Therefore, a helical strake was used to reduce vortex shedding vibrations.

Depending on the geometry the use of helical strakes can reduce vortex shedding oscillation by about 98% [23] and they can be easily designed and implemented as well. A helical strake was used to cover 45% of the steel stack height from the top to decrease the lateral displacement below the limit stated in the Eurocode 3. Therefore, by employing a helical strake, the effect of vortex shedding was reduced, and the lateral top displacement caused by the vortex shedding decreased by approximately 5 times, as shown in Table 3. The maximum lateral top displacement of the stack along its height was obtained from wind loads before the use of helical strakes (WDWOHS), displacement due to wind loads after the use of helical strakes (WDWHS) and displacement due to earthquake loads (ED) curves were obtained and were shown in Fig. 3. As can be seen from Fig. 3, wind is more effective than earthquake during design.

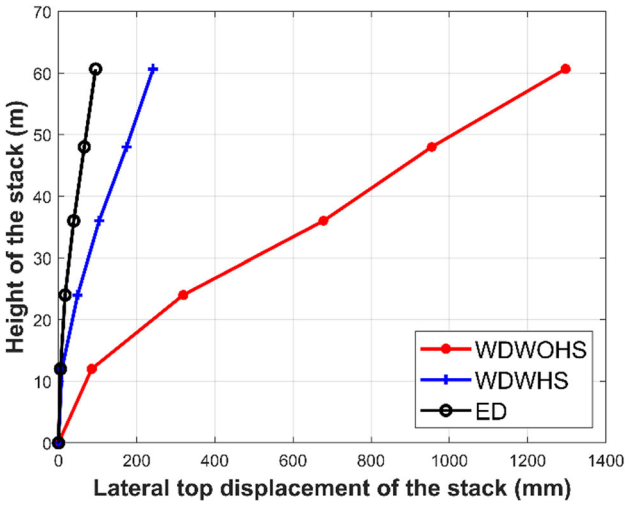

Fig. 3 The lateral top displacements along the height of the stack

Table 4 Demand-to-capacity ratio for beam-columns

	Load combination	Codes	DCR
Without helical strake	$G + W_{across}$	TCDCSS 2016	2.49
	$G + Q + W_{across}$	ASME STS-1	2.44
With helical strake	$G + W_{across}$	TCDCSS 2016	0.65
	$G + Q + W_{across}$	ASME STS-1	0.44

The base shear force in the cross-wind direction also decreased from 1683.22 to 280.04 kN. As can be seen in Table 3, the demand displacements obtained from the analyzes using the load combinations stated in TCDCSS 2016 and ASME STS-1 are quite compatible with each other. Furthermore, the steel stack was considered as a cantilever element and the maximum lateral top displacement of the stack under seismic load was limited to $\Delta_{max} = h/150 = 60650/150 = 404$ mm in its design.

The requirements for the strength limit states according to TCDCSS 2016 and ASME STS-1 were also satisfied. The check of the strength limit state in the most critical segment for longitudinal compression and bending combination is shown in Table 4. Since the requirements stipulated in TCDCSS 2016 depend on the demand/capacity ratio for beam-columns, the demand/capacity ratio (DCR) has been checked for the both regulations. Demand/capacity ratio (DCR) is the ratio of the required flexural strength to the available flexural strength for beam-columns. As can be seen in

Table 4, the demand-to-capacity ratio decreased below unity (1.00) with the use of helical strakes.

The demand-to-capacity ratio of 0.03 for the most critical segment for the local buckling limit state was below unity (1.00). Therefore, the local buckling limit state also satisfied in design stage for each segment of the steel stack according to the formula suggested by Troitsky.

3 Finite Element (FE) Analysis

The nonlinear behavior and seismic performance of the steel stack has been investigated by conducting the nonlinear time history and the static pushover analyses of finite element models developed by using ABAQUS/Explicit software.

Eleven ground motions were selected for the nonlinear time history analyses in accordance with the TSCB 2018. The data bases of the Disaster and Emergency Management Presidency of Turkey (DEMP) [24] and the Pacific Earthquake Engineering Research (PEER) [25] Center were used for selection of the ground motions. The information of the selected acceleration records is given in Table 5.

Scaling of the record with respect to the design spectrum was accomplished in the range of $0.2T_p$–$1.5T_p$ for the one-dimensional response of the eleven earthquake ground motion records in accordance with the TSCB 2018, where T_p (0.82 s) denotes the first natural vibration period of the stack. The scale factors for each earthquake record are given in Table 6.

The elastic response spectra of the eleven scaled records and the mean of these spectra with the selected design spectrum were presented in Fig. 4. It is clear that the average spectrum remains above the design spectrum within the desired range.

3.1 Material Model

The steel grade of S235 was preferred as the material with an elastic modulus of $E = 200$ GPa and Poisson's ratio of 0.30. The strain-hardening was also considered for FE model (Fig. 5). The strain at the beginning of the strain-hardening was accounted for as $\varepsilon_s = 11\varepsilon_y$, and at the failure is $\varepsilon_u = 120\varepsilon_y$ based on the study of Baei et al. [26].

Isotropic hardening model was implemented in the numerical analysis because the growth of yield surface in the multi-dimensional stress is well-represented by this model. However, since longitudinal bending stresses are very effective compared to other stresses, these stresses have also been effective in plasticization, and it is expected that the isotropic hardening model will still represent the yielding and plastification well.

Table 5 The selected acceleration records

Order	Record information	Direction	PGA (g)	Abbreviation of record
1	Afyon Turkey, 03/02/2002	NS	0.096	AFYON
2	Erzincan Turkey, 13/03/1992	EW	0.496	ERZINCAN1
3	Erzincan Turkey, 13/03/1992	EW	0.489	ERZINCAN2
4	Kocaeli Turkey, 17/08/1999	NS	0.364	KOCAELI1
5	Kocaeli Turkey, 17/08/1999	NS	0.233	KOCAELI2
6	Duzce Turkey, 12/11/1999	EW	0.515	DUZCE1
7	Duzce Turkey, 12/11/1999	EW	0.822	DUZCE2
8	Bingol Turkey, 01/05/2003	NS	0.511	BINGOL
9	Denizli Turkey, 01/10/1995	EW	0.327	DENIZLI
10	Elazig Turkey, 24/01/2020	EW	0.298	ELAZIG
11	Mugla Turkey, 20/07/2017	NS	0.161	MUGLA

Table 6 Scale factors

Order	Abbreviation of record	Scale factors
1	AFYON	5.00
2	ERZINCAN1	1.25
3	ERZINCAN2	1.29
4	KOCAELI1	1.45
5	KOCAELI2	2.36
6	DUZCE1	1.06
7	DUZCE2	0.91
8	BINGOL	1.46
9	DENIZLI	1.45
10	ELAZIG	1.77
11	MUGLA	3.37

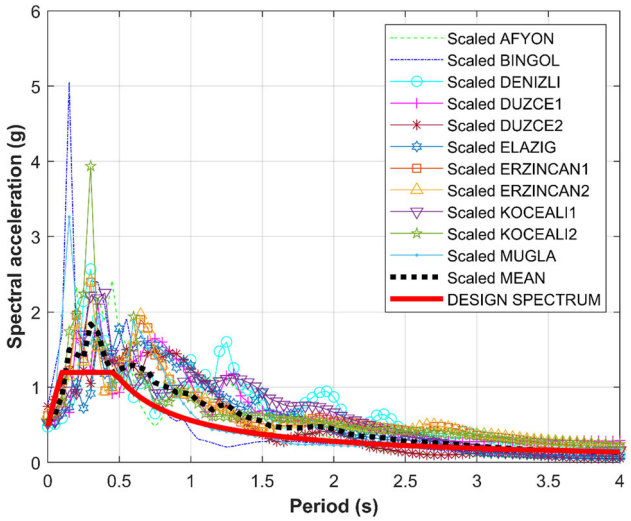

Fig. 4 Scaled records and the selected design spectrum

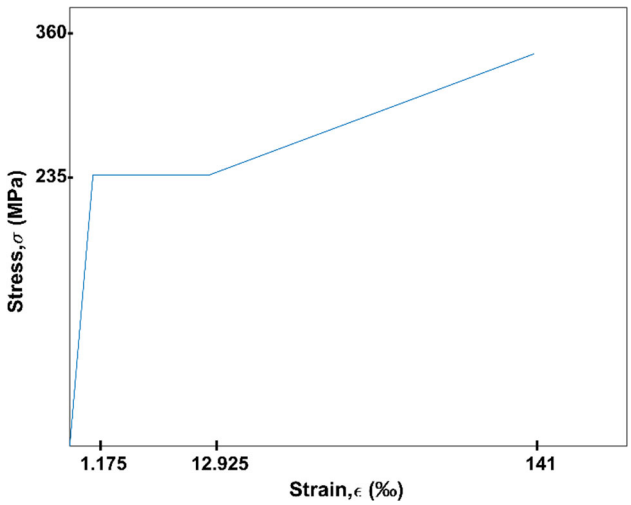

Fig. 5 Stress–strain curve for the steel material of the steel stack

3.2 Finite Element Model (FEM)

The stack consists of five individual segments. It was assumed that all splice steel connections provide sufficient resistance and thereby, the forces and the moments were transferred safely by the elements in the splice connections.

Basically, shell elements with 4-node doubly curved thin or thick shell such as S4R were used for nonlinear time history analyses. In order to avoid convergence problems and to obtain acceptable accuracy, the members of the stack were modeled so as to form a square element with edge size of 0.50 m.

The connections between the segments of the steel stack were provided by means of the flange plates and bolts. The base plate of the stack was connected to the foundation by anchor rods. Both connections were not explicitly included in the FE model. The boundary condition at the base was assumed to be directly fully fixed. The mass of the platforms was modeled as a rigid coupling connecting the levels of 41.00 m and 58.65 m where the platforms were located.

The effect of damping in the dynamic analysis is included by adopting Rayleigh damping model proposed by Chopra [27]. The damping coefficients proportional to the mass and stiffness of the steel stack were determined for a damping ratio of 2% using the first and third natural frequencies. These coefficients used in the numerical analysis are $\alpha_0 = 0.2443$ and $\alpha_1 = 0.0009268$, respectively.

In Rayleigh damping, the damping matrix (C) is the linear combination of the mass matrix (M) and stiffness matrix (K) and is expressed by the following equation;

$$C = \alpha_0 M + \alpha_1 K$$

where α_0 and α_1 are the mass and stiffness matrix coefficients, respectively, and are calculated depending on the natural frequencies by the following equations:

$$\alpha_0 = \xi \frac{2\omega_i \omega_j}{\omega_i + \omega_j}, \quad \alpha_1 = \xi \frac{2}{\omega_i + \omega_j}$$

where ω_i and ω_j are the natural frequencies for the ith and jth modes, respectively, and ξ is the damping ratio of these modes.

The stack was also modeled with 8-node linear brick elements (C3D8) for nonlinear static pushover analysis. The finite element meshes in the first 1/5 of the height from the base were modeled by using a square element with a side size of 0.10 m and in the other parts with a side size of 0.20 m in the solid element. Four mesh layers of elements were used through the thickness of the parts in the model in order to represent the bending effects well, possible local buckling of the stack wall and to obtain realistic results. For the performance evaluation of the stack, the expected yield strength, $R_y F_y$ ($R_y = 1.4$) and expected tensile strength, $R_t F_u$ ($R_t = 1.1$) were considered for the steel material of S235 according to the TSCB 2018.

The effect of the flue opening on the strength and the lateral stiffness of the stack was also investigated. Figure 6 shows the steel stack with flue openings, FE models with and without flue openings. A prismatic opening with dimensions of 2.0 m × 4.0 m at 6.0 m height from the base and 1.0 m × 1.2 m at 10.0 m height from the base and circular opening of 1.20 m in diameter at 20.0 m above the base were provided in the steel stack. These openings were provided in different directions of the stack and stiffeners were used around the openings.

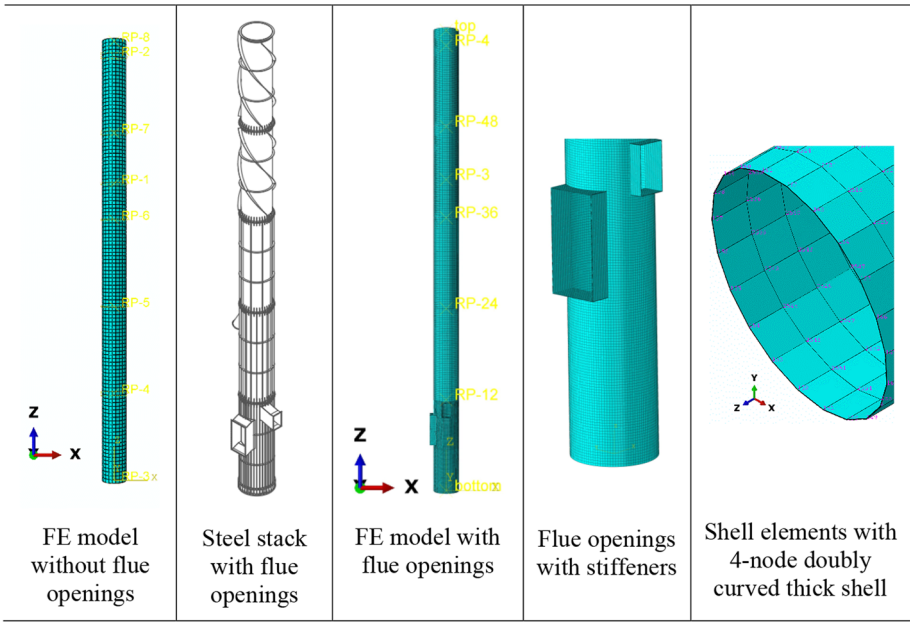

Fig. 6 Finite element models of the stack with and without flue openings

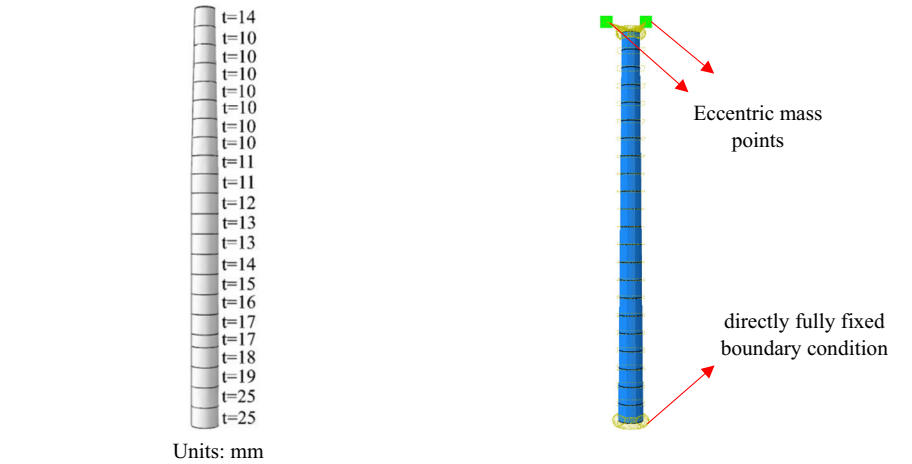

(a) Wall thickness of the wind turbine (b) FE model of the wind turbine

Fig. 7 The geometry and FEM of the wind turbine

3.3 Verification of Finite Element Model

The studies conducted by Dai et al. [28] and Xu et al. [29] were used to verify the finite element model established for the sample steel stack. In this studies, 15 MW horizontal-axis wind turbine with a hub height of 65.0 m was considered. The natural frequencies of the wind turbine were measured and its performance under lateral forces was investigated by performing the nonlinear time history. For the steel material used, yield strength, elastic modulus, Poisson's ratio and density were taken as 345 MPa, 206 GPa, 0.3 and 7850 kg/m^3, respectively. The outer diameter of the wind turbine increases along its height, being 4.035 m at the base and 2.955 m at the top. The geometry of the wind turbine modeled as 22 segments with different wall thicknesses is shown in Fig. 7a.

ABAQUS software was used for creating the finite element model of the wind turbine. The position of the masses of the hub and nacelle were considered by placing two eccentric mass points, with masses of 15 tons and 60 tons with the eccentricity of 2.5 m and 1.0 m respectively, from the top of tower. The boundary condition at the bottom of the wind turbine FE model was directly fully fixed as shown in Fig. 7b and the mass of hub and nacelle were modeled as a rigid coupling connecting to the top of the tower.

The natural frequencies and mode shapes were obtained based on Lanczos method in the ABAQUS software. The field measured values of a real 1.5 MW wind turbine tower obtained by Dai et al. and the values of the first three order natural frequencies determined from the FE model are compared in Table 7. Only the first two order natural frequencies could

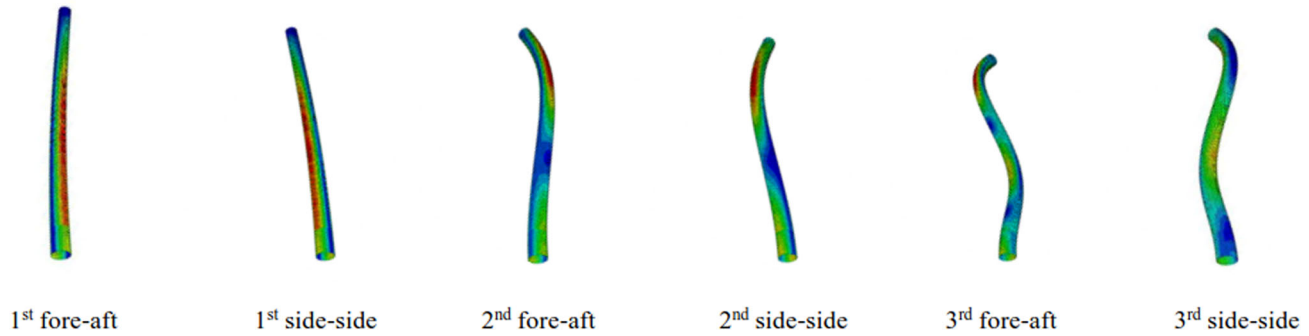

Fig. 8 Mode shapes of the wind turbine model

Table 7 Frequency of the wind turbine

Mode order	Frequency (Hz)	
	FE Model	Measured value
1st fore-aft	0.460	0.490
1st side-side	0.459	0.480
2nd fore-aft	3.989	3.850
2nd side-side	4.175	4.080
3rd fore-aft	11.900	–
3rd side-side	12.087	–

be determined in the field studies. The directions perpendicular to the blades and parallel to the blades were adopted as the "fore-aft direction" and "side-side direction," respectively, as in the study of Xu et al. Moreover, the first three natural mode vibrations of the wind turbine are shown in Fig. 8.

The linear time history analysis was performed based on the information obtained from the research considered. The horizontal displacement at the tower top of the wind turbine was obtained by using the ground motion acceleration records from the station named TCU052E for the Chi-Chi, Taiwan earthquake. The time–displacement curve in the study conducted by Xu et al. and the curve obtained in the current study are shown in Fig. 9.

The consistency of the first two natural frequencies and vibration modes obtained from the FE model with the field measured values verify the validity of the model. Furthermore, comparison of as the time–displacement curves shows good agreement with the results in study of Xu et al. The slight difference between results is attributed to the simplifications and assumptions in the FE model. Consequently, the FE model assumed to be applicable for the simulation of the steel stack models under the nonlinear time history and the static pushover loading.

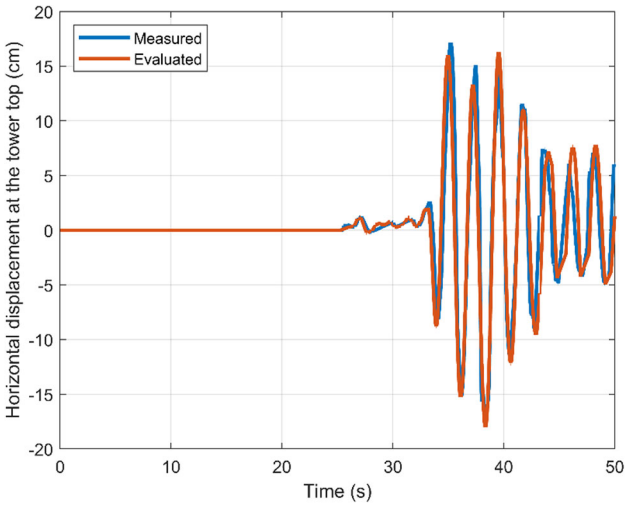

Fig. 9 The comparison of time–displacement curves of seismic responses

3.4 Finite Element Analysis Results

The first-four vibration modes of the FE models with the shell elements (Model A), the model without a flue opening (Model B) and that with solid elements including flue openings (Model C) were shown in Figs. 10, 11, 12, respectively. Natural vibration periods were also shown in Table 8 collectively. It is seen that the vibration periods of Model A and Model B are close to each other, while the periods of Model C are slightly larger due to the decrease in lateral stiffness.

3.5 Seismic Response of the Steel Stack

The maximum lateral top displacements of the stack were obtained from the nonlinear time history analyses. The displacements along the height, their mean values, 10% increased mean values and the displacement limit are shown in Fig. 13.

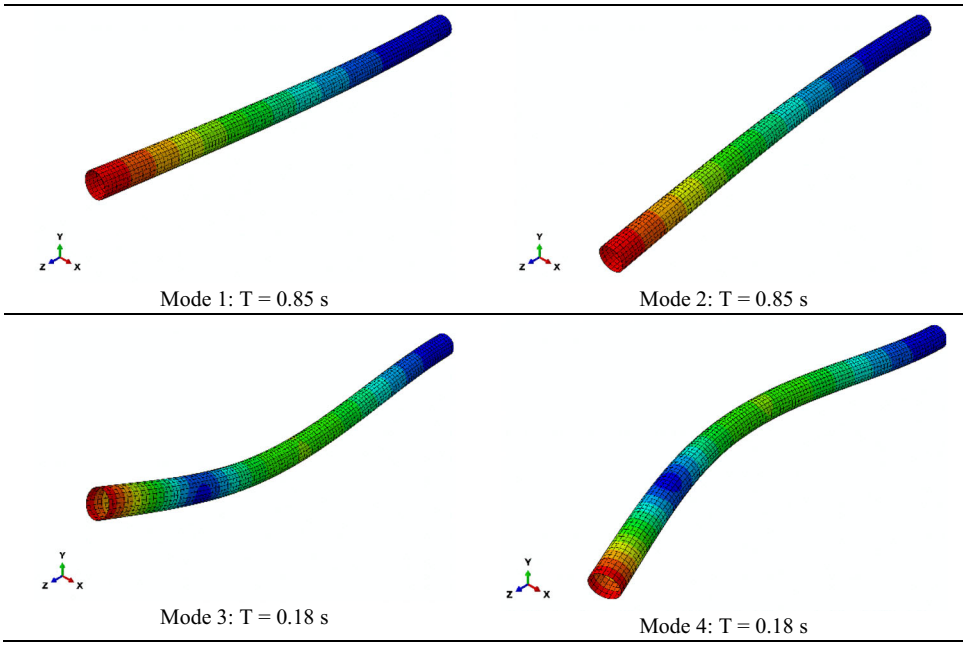

Fig. 10 Vibration modes of the Model A

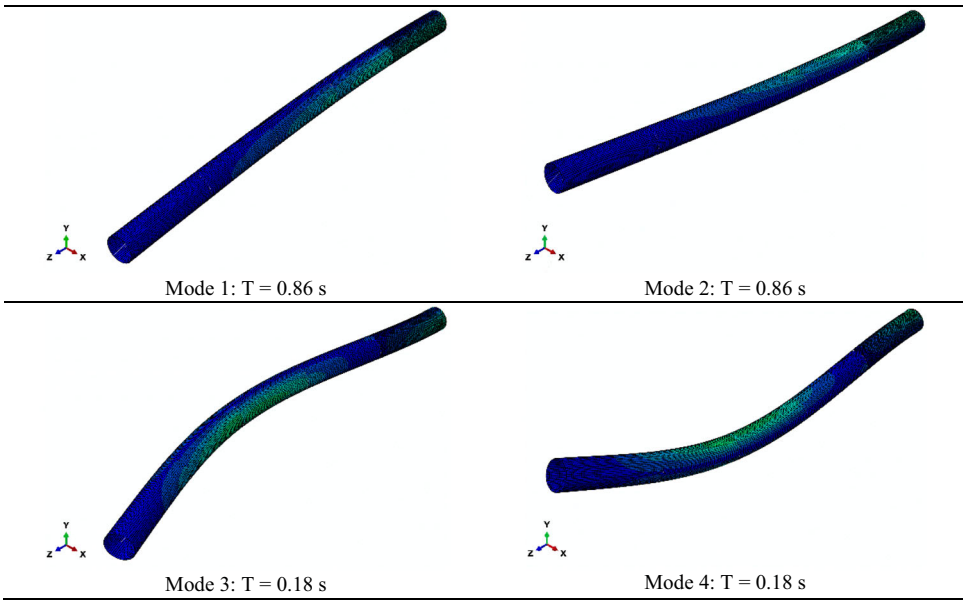

Fig. 11 Vibration modes of the Model B

It is clear that even the 10% increased mean displacement under ground motions remains below the limit adopted initially. Therefore, the steel stack designed to prevent vortex shedding vibration also satisfies the requirement for displacement under earthquakes.

Yielding at two critical heights along the stack (the base and the splice at a height of 24.0 m from the base) was also investigated. Under the seismic ground motions, the levels where the largest strains occurred along these critical heights were determined and the strains occurred during the earthquake at these levels were obtained. This process was repeated for each earthquake ground motion records. It was observed that the largest strains occur at the base and at the splice at a height of 24.0 m from the base, as shown in Fig. 14. While the first mode was effective in earthquakes where the largest strain occurred at the base, higher modes were effective in earthquakes where the strain was the largest at a height of 24.0 m from the base. Normalized strain ($\varepsilon/\varepsilon_y$) at these levels was obtained in such a way that the largest of the stack strain (ε) divided by the yield strain of the steel (ε_y). As seen in Fig. 15, the yield limit is not exceeded along the stack, so the strain is in the elastic zone and no plastic strain occurs. It shows that the stack can exhibit excellent performance under seismic ground motions.

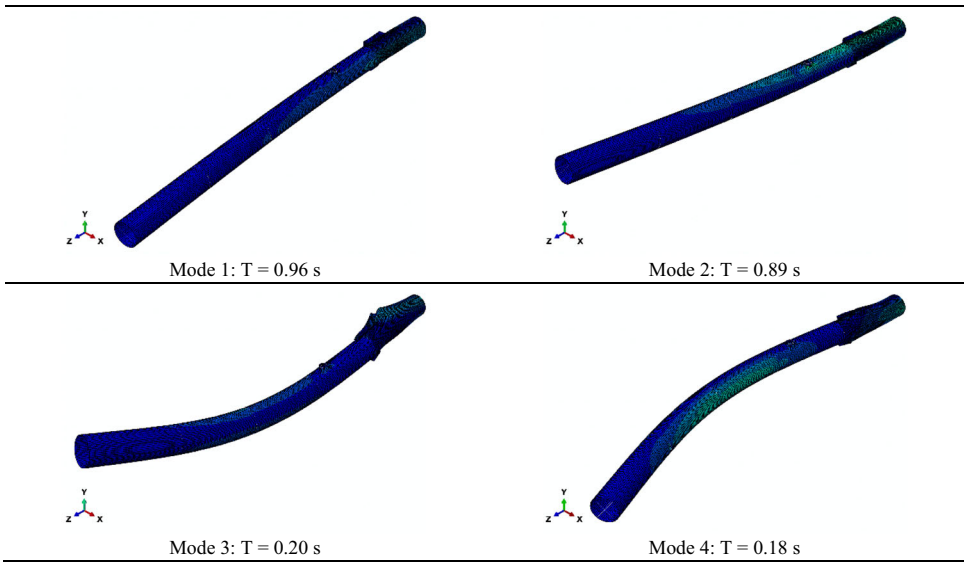

Fig. 12 Vibration modes of the Model C

Table 8 Natural vibration periods of FE models

Model	1st Mode (s)	2nd Mode (s)	3rd Mode (s)	4th Mode (s)
Model A	0.85	0.85	0.18	0.18
Model B	0.86	0.86	0.18	0.18
Model C	0.96	0.89	0.20	0.18

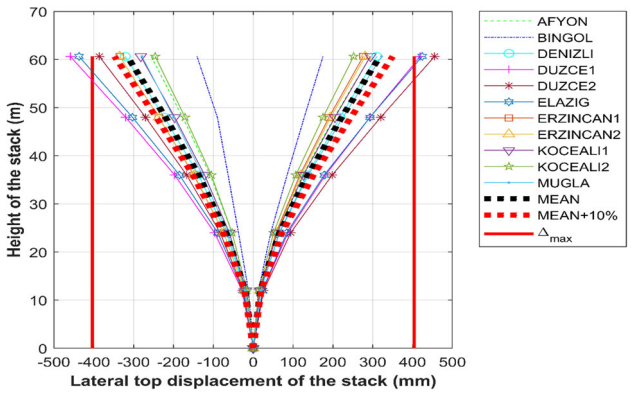

Fig. 13 The maximum lateral top displacements along the height of the stack

3.6 The Effect of Flue Opening on the Strength and Lateral Stiffness of the Steel Stack

The flue opening is usually provided for the entrance and to exit of flue gases, maintenance and regular checking process. In order to investigate the effect of the flue opening on the strength and the lateral stiffness, the capacity curves were obtained by using the expected materials strength for the stack with the flue opening (PWFO) and without the flue opening (PWOFO) and displayed in Fig. 16.

As can be seen in Fig. 16, the presence of the flue opening caused decrease in the strength and the lateral initial stiffness of the stack by about 13% and 18%, respectively, which required to be considered in the design. It is also appropriate to use stiffeners for reinforcing the openings in order to prevent local yielding that may cause more significant decrease in lateral stiffness due to stress concentrations which occur around these openings, as shown in Fig. 17. The stresses around the opening exceeded the expected yield strength of 329 MPa by 28% and inelastic deformations occurred. Plastic strains would likely to spread over a wider area, if the stiffener around the opening was not used.

3.7 Performance Assessment of the Steel Stack

Base shear forces are shown on the capacity curve of the stack obtained by using the nominal materials strength (Fig. 18). $V_{t,\mathrm{RSM}}$ and $V_{t,\mathrm{EELM}}$ indicate the elastic base shear forces obtained by the response spectrum method and by the equivalent earthquake load method, respectively. $V_{t,\mathrm{AW}}$ and $V_{t,\mathrm{CW}}$ denote the base shear forces obtained in the along-wind direction and in the cross-wind direction, respectively. $V_{t,\mathrm{NTH}}$ indicates the mean of the largest base shear forces obtained by nonlinear time history analysis.

The base shear force due to seismic load was slightly higher (approximately 3%) than that due to wind load; however, wind loads created maximum lateral displacement at the

Fig. 14 The levels where the largest strain occurred along the stack

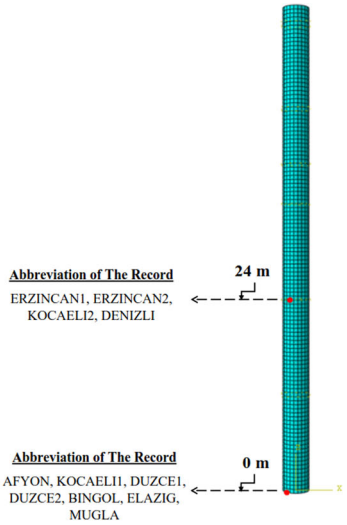

(a) The levels where the largest strain occurred for all seismic ground motions

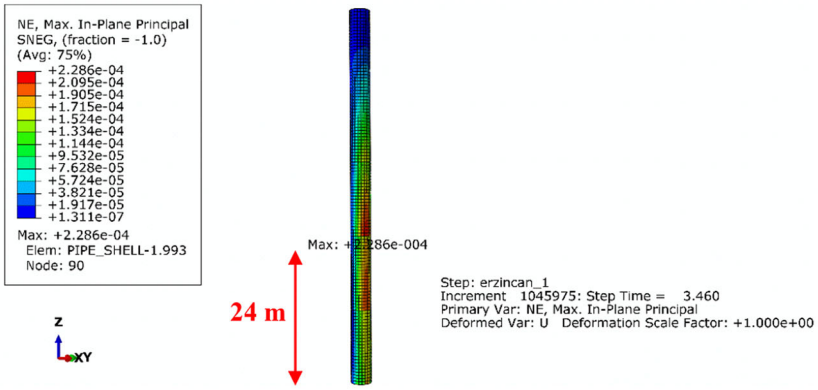

(b) The level where the largest strain occurred for ERZINCAN1

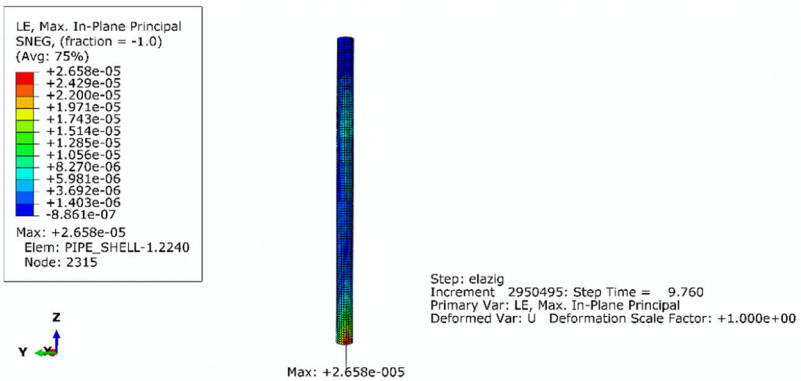

(c) The levels where the largest strain occurred for ELAZIG

top of the stack. Therefore, the wind loads were more pronounced than earthquake in design stage. Although the steel stack was designed to prevent vortex shedding vibrations, the base shear likely to be occurred during the earthquake was below the nominal capacity of the stack, as seen in Fig. 18.

The capacity of the stack reached 922.0 kN when the lateral top displacement was achieved as 2.1 m, as seen in Fig. 18. After this point, local out-of-plane deformations (local buckling) occurred at the bottom of the stack and the capacity started to decrease.

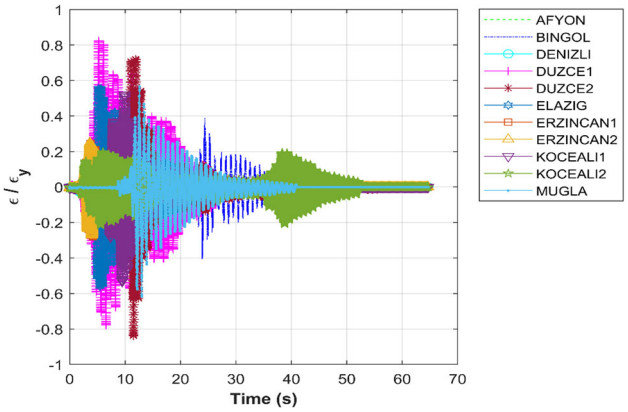

Fig. 15 Time variation of the largest normalized strain with respect to the yield strain

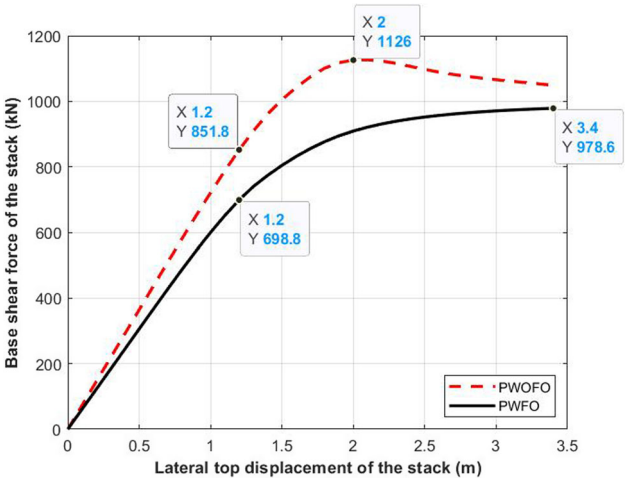

Fig. 16 Pushover curves of the stack to show the effect of flue opening

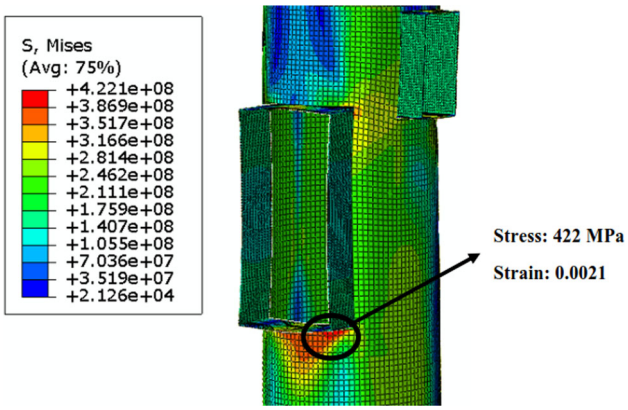

Fig. 17 Stress concentrations around flue opening

Wind loads are often more critical than seismic loads in the design of tall structures, as seen in this study, due to their specific dynamic nature, although it depends on the region where the structure will be built. For such stacks which the wind loads are more pronounced in the design stage and when the lateral top displacement is particularly limited to (h/150), the seismic response of the steel stack cantilevered from the base remains in elastic level as expected from the structures statically determined. Moreover, when the mean of the largest base shear force obtained by the nonlinear time history analysis, shown in Fig. 18, was considered as required base shear strength met by the stack, it was demonstrated that plastic strain did not occur at any point over the stack.

4 Conclusions

A sample self-supporting steel stack is designed considering the international standards, codes and specifications. Nonlinear behavior and seismic performance of the stack are investigated by using nonlinear analyses. The principles used for the design of the steel stack have been specified as intended initially. The requirements to be considered in the design of a steel stack are also explained parallel to these principles.

The following conclusions can be drawn based on the present study including a sample stack.

1. The wind loads are found to be more pronounced compared to seismic forces in the design of the self-supporting steel stack.
2. Limiting the peak displacement is the governing criterion for the design of the self-supporting steel stack. Therefore, measures to reduce displacement should be taken at the design stage.
3. To limit the horizontal top displacement at $h/150$ is found applicable in both along-wind and across-wind direction directions. Therefore, the value of $h/150$ may be used as a limiting value in the design of self-supporting steel stacks under lateral loads.
4. A self-supporting steel stack designed according to wind loads remains safe without any plastic deformation under the expected strength demand during an earthquake.
5. The presence of flue openings reduces the lateral stiffness and strength of steel stack. The stresses concentrate around these openings and exceed the expected yield strength of 329 MPa by 28%. Therefore, it is appropriate to use stiffeners around the opening in order to prevent stress concentrations that occur around these openings and a significant decrease in lateral stiffness.
6. The use of helical strakes reduce vortex shedding oscillation by approximately five times. Therefore, the demand-to-capacity ratio for each segment of the stack is well

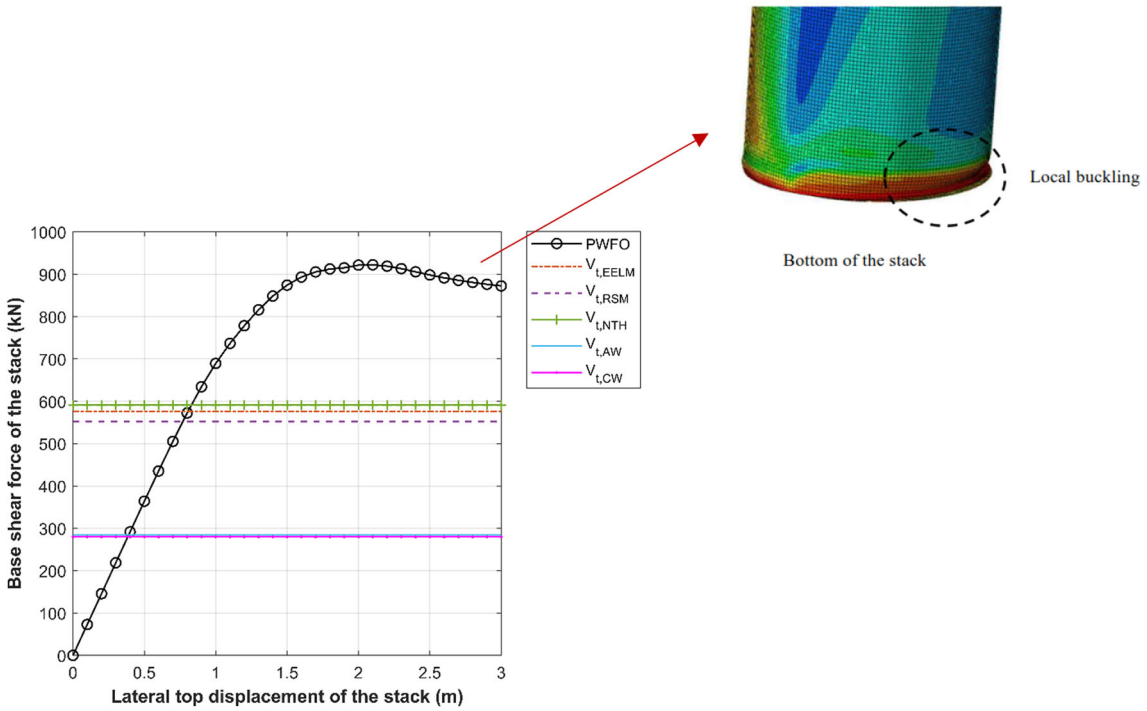

Fig. 18 Capacity curve and local buckling of the steel stack

below unity (1.00) and no plastic behavior is detected along the stack in the earthquake analysis.

The study is limited to the design and nonlinear analyses of a typical self-supporting steel stack to evaluate its performance. More studies should be done on this subject and it is also necessary to investigate the dynamic response of steel stacks to the wind effects as in the earthquake.

Funding Open access funding provided by the Scientific and Technological Research Council of Türkiye (TÜBİTAK).

References

1. Gaczek, M.; Kawecki, J.: Analysis of cross-wind response of steel chimneys with spoilers. J. Wind Eng. Ind. Aerodyn. **65**(1–3), 87–96 (1996). https://doi.org/10.1016/S0167-6105(97)00025-1
2. Kawecki, J.; Zurański, J.A.: Cross-wind vibrations of steel chimneys—A new case history. J. Wind Eng. Ind. Aerodyn. **95**(9–11), 1166–1175 (2007). https://doi.org/10.1016/J.JWEIA.2007.02.001
3. Eurocode 1, "EN 1991–1–4. Eurocode 1: Actions on Structures, Part 1–4: General Actions-Wind Actions." European Committee for Standardization, Brussels, Belgium, (2005)
4. CICIND, "Model Code for Steel Stacks, Revision 2." International Committee on Industrial Stacks, Germany, (2010)
5. Susuki, T.; Hanada, N.; Homma, S.; Maeda, J.: Wind-induced vibration control of a 200 m-high tower-supported steel stack. Wind Struct. **9**(5), 345–356 (2006). https://doi.org/10.12989/was.2006.9.5.345
6. Huang, W.; Gould, P.L.; Martinez, R.; Johnson, G.S.: Non-linear analysis of a collapsed reinforced concrete chimney. Earthq. Eng. Struct. Dyn. **33**(4), 485–498 (2004). https://doi.org/10.1002/eqe.362
7. ABAQUS, "Analysis User's Guide." Hibbit, Karlsson, and Sorenson, Inc, RI, USA (2017)
8. ABAQUS, "Getting Started with ABAQUS: Interactive Edition." Hibbit, Karlsson, and Sorenson, Inc, RI, USA, (2017)
9. Wilson, J.L.: The cyclic behaviour of reinforced concrete chimney sections with and without openings. Adv. Struct. Eng. **12**(3), 411–420 (2009). https://doi.org/10.1260/136943309788708329
10. ASME STS-1, "Steel Stacks." The American Society of Mechanical Engineers, New York, USA, (2011)
11. Eurocode 3, "EN 1993–3–2. Eurocode 3: Design of Steel Structures - Part 3–2: Towers, Masts and Stacks- Stacks." European Committee for Standardization, Brussels, Belgium, (2006)
12. IS 6533, "Code of Practice for Design and Construction of Steel Stack: Part 2 Structural Aspect, First Revision." Bureau of Indian Standards, New Delhi, India, (2002)
13. ASCE 7–16, "Minimum Design Loads for Buildings and Other Structures." American Society of Civil Engineers, Reston, Virginia, USA, (2016)

14. AISC 360–16, "Specification for Structural Steel Buildings." American Institute of Steel Construction, Chicago, Illinois, USA, (2016)
15. SAP2000, "Integrated Software for Structural Analysis and Design V20.2." Computers and Structures Inc., Berkeley, California, USA, (2020)
16. Kültür, Ö.F.; Al-Masri, A.; Sayin, B.: Effect of high temperature exposure on design parameters and collapse behavior of reinforced concrete and steel-framed buildings. Case Stud. Const. Mater. **17**, e01263 (2022). https://doi.org/10.1016/j.cscm.2022.e01263
17. ASCE, "Design and Construction of Steel Stack Liners." American Society of Civil Engineers, New York, USA, (1975)
18. TSCB 2018, "Turkish Seismic Code for Buildings." Disaster and Emergency Management Presidency, Ankara, Turkey, (2018)
19. AIJ, "Recommendations for Loads on Buildings." Architectural Institute of Japan, Japan, (2015)
20. Troitsky, M. S.: Tubular Steel Structures: Theory and Design, 2nd edn. Arc Welding Foundation, USA (1990)
21. TCDCSS 2016, "Turkish Code for Design and Construction of Steel Structures 2016." Ministry of Environment and Urbanization, Ankara, Turkey, (2016)
22. AISC, "Steel Construction Manual, 15th edition." American Institute of Steel Construction, Chicago, Illinois, USA, (2017)
23. Zhou, T.; Mohd, S.F.; Razali, Z.H.; Cheng, L.: On the study of vortex-induced vibration of a cylinder with helical strakes. J. Fluids Struct. **27**(7), 903–917 (2011). https://doi.org/10.1016/j.jfluidstructs.2011.04.014
24. DEMP, "Turkey Seismic Hazard Map." Disaster and Emergency Management Presidency, Ankara, Turkey, (2020)
25. PEER, "Ground Motion Database." Pacific Earthquake Engineering Research Centre, Berkeley, CA: University of California, USA, (2020)
26. Baei, M.; Ghassemieh, M.; Goudarzi, A.: Numerical modelling of end-plate moment connection subjected to bending and axial forces. J. Math. Comput. Sci. **04**(03), 463–472 (2012). https://doi.org/10.22436/jmcs.04.03.21
27. Chopra, A.K.: Dynamics of Structures: Theory and Applications to Earthquake Engineering, 5th edn. Pearson, London (2020)
28. Dai, K.; Huang, Y.; Gong, C.; Huang, Z.; Ren, X.: Rapid seismic analysis methodology for in-service wind turbine towers. Earthq. Eng. Eng. Vib. **14**(3), 539–548 (2015). https://doi.org/10.1007/s11803-015-0043-0
29. Xu, Y.; Ren, Q.; Zhang, H.; Shi, W.: Collapse analysis of a wind turbine tower with initial-imperfection subjected to near-field ground motions. Structures **29**, 373–382 (2021). https://doi.org/10.1016/j.istruc.2020.11.019